Static Analysis and Dimensional Optimization of a Cable-Driven Parallel Robot

Matthew Newman(✉), Arthur Zygielbaum, and Benjamin Terry

Department of Mechanical and Materials Engineering,
University of Nebraska – Lincoln, Lincoln, NE, USA
mbnewman91@gmail.com

Abstract. A cable-driven parallel manipulator has been chosen to suspend and navigate instruments over a phenotyping research facility at the University of Nebraska. This paper addresses the static analysis and dimensional optimization of this system. Analysis of the system was performed with catenary simplification to create force equilibrium equations and define a mathematical model. The model incorporates flexibility due to catenary sag of the cables. Cable axial stiffness was not included because stiffness is dominated by catenary flexibility for the expected cable tensions. The model was used to optimize system dimensions, and a twelfth-scale system was constructed to verify the model as well as enable dynamic and control system experimentation during full-scale system construction. Miniature end-effectors were used to obtain end-effector orientation and cable tension measurements which were comparable to model predictions. The mathematical model was thereby shown to be accurate for the purpose of system static analysis.

Keywords: Parallel machines · Robot kinematics · Modeling · Manipulator motion-planning

1 Introduction

1.1 Motivation

Agricultural productivity is dependent on the development of crops which can meet certain requirements such as resilience in the face of environmental or pest stressors, or a level of productivity (yield) despite restrictions in nutrients or water. Breeding such crops is an iterative process where the result of crossing the genes of sets of plants causes measureable changes in successive generations. These changes are determined by measuring the plants phenotypes – observable characteristics. Phenotyping in a greenhouse can now be done rapidly using automated equipment. Greenhouse plants, however, are different from plants grown in a field environment. Light conditions are different. Soils are less uniform. And wind does not encourage the growth of support structure within the plants. Assuring that measurements in a greenhouse are trustworthy predictions of field performance is the holy grail of phenotyping. To this end, a field rapid phenotyping system is being developed at the University of Nebraska-Lincoln's Agricultural Research and Development Center. The system described in this paper is designed to position

C. Gosselin et al. (eds.), *Cable-Driven Parallel Robots*,
Mechanisms and Machine Science 53, DOI 10.1007/978-3-319-61431-1_14

instruments precisely over research plots in order to rapidly and repeatedly make phenotypic measurements of sets of plant varieties and experimental treatments.

1.2 Cable-Driven Parallel Robots

A cable-driven parallel robot (CDPR) is a robotic manipulator designed to control the position and/or orientation of its end-effector within the system's workspace by use of actuated cables. CDPRs provide several benefits over traditional rigid-leg serial and rigid-leg parallel manipulators in the study of crop phenotyping. CDPRs offer minimal interference with the crops compared to rigid-support systems. Traditional serial or parallel manipulators interfere with plant growth because they are composed of large supports and machinery which reflect and obstruct light and air flow. In addition, CDPRs are generally lighter and therefore capable of greater accelerations while maintaining high energy efficiency compared to rigid-linkage robots [1]. However, CDPRs have several design challenges. Cables can only perform while in tension, which puts limitations on end-effector position and greatly influences positional accuracy and system vibrations [2, 3].

CDPRs can be broken into three basic categories based on the number of cables and the mobility of the system: fully constrained, under constrained, and over constrained. A fully constrained parallel robot requires at least one more cable than the degrees of freedom of the end effector. In the case of three-dimensional translational motion, as is the focus of this paper, a fully constrained system requires four cables for full control of position. The number of cables can be reduced if a constant external force, such as gravity, is applied to the end-effector. This force acts as an additional cable on the end-effector, reducing the number of physical cables needed to fully constrain the system [1].

This paper focuses on the suspended four-cable parallel robot. In these systems, the end-effector is supported by four cables with gravity delivering a downward force on the end-effector, behaving as a fifth cable. The four-cable configuration is beneficial over three-cable systems as the same system footprint has an expanded available workspace and the cable load is reduced by distributing the load to an additional cable. However, using four cables creates a redundancy in the support system and complicates the system modeling and control as no unique cable configuration exists for an arbitrary location in the workspace [1].

Further modeling and design considerations come from the scale of the CDPR. In many CDPRs, cables can be assumed to have negligible mass, greatly simplifying system modeling and control. However, in the case of large-scale systems, cable weight can induce catenary sag in the cables which strongly influences positional accuracy as well as system dynamics and vibration.

Significant work has been accomplished in the area of CDPRs, including kinematic design [1, 2, 15, 16] and dynamic analysis [3–7]. Additionally, a large amount of research has been conducted in the area of cable mechanics [6, 8–10]. However, limited research exists in the field of large-scale suspended CPDRs where cable sag can play a major role in system dynamics and control. One of the few examples of research into the area of cable sag in cable-driven manipulators is the FAST telescope, a newly constructed five hundred meter CDPR in China [11].

1.3 Objective

Substantial research has been performed by the FAST project on vibrations and stabilization of large scale CDPRs. However, the high speed requirements of the phenotyping system and the proportionally lower weight end-effector and cables results in significantly different system requirements and dynamics for a phenotyping system with four cables. The objective of this research is to develop a CDPR design and control scheme that can autonomously and rapidly move between crop plots. This system must be functional during harsh weather conditions, pass through the crop canopy with minimal crop interference, and provide stability for the phenotyping sensors mounted on the end-effector. The purpose of this paper is to present a static model of the system as a first step to aid future system design optimization and dynamic modeling of a CDPR for crop phenotyping. In addition, a scaled-down system is built to gather experimental results and confirm the validity of the theoretical models developed.

This paper focuses on computing the inverse kinematics and verifying these results experimentally. The solution begins with an analysis of a single cable to obtain the cable profile and tension. This solution then determines the force equilibrium equations for the four-cable system supporting a point-mass end-effector. The resulting force vectors are then applied to the end-effector model using the moment equilibrium equations to determine the orientation of the end-effector. In order to simplify calculations, cables are assumed to be inextensible due to low tension values predicted in the cables compared to their elastic modulus and the predicted dominance of cable sag on cable flexibility [9].

Until construction of the full-scale system is complete, drive and control systems tests are performed using a scaled system. Vibrations and stability of the scaled system are not thoroughly investigated due to scaling incompatibilities between the test platform and the full-scale system. Because of the difficulties associated with scaling cable properties, the dynamic experimentation is assumed to not scale to the full-scale system. As such, controls tests and system properties including system stiffness and vibration predictions are not discussed in this paper.

2 Simulation

2.1 Geometric Analysis

In flexible cables with significant mass, the weight of the cable provides varying vertical load along the length of the cable which generates a curve as defined by (1) and is illustrated by Fig. 1 [12].

$$y = A * \cosh\left(\frac{x}{A}\right) \tag{1}$$

Where A is the relationship between the constant horizontal tension seen in the cable (Th) and the linear weight of the cable (w) (Fig. 2).

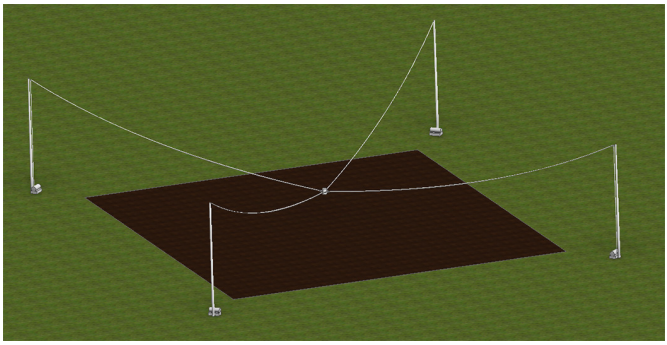

Fig. 1. Conceptual model of phenotyping system.

$$A = \frac{T_h}{w} \tag{2}$$

Cable length (S) can then be calculated based on the arc length formula, integrating from cable end points, (x_1,y_1) and (x_2,y_2).

$$S = \int_{x_1}^{x_2} \sqrt{1 + \left(\frac{dy}{dx}\right)^2}\, dx = A * \sinh\left(\frac{x_2}{A}\right) - A * \sinh\left(\frac{x_1}{A}\right) \tag{3}$$

The cable angle at any point along the cable (Ψ) can also be solved geometrically as,

$$\tan(\Psi) = \frac{dy}{dx} = \sinh\left(\frac{x}{A}\right) \tag{4}$$

Provided that a cable can only experience axial load, at any point along the cable, tension (T) must be tangent to the cable curvature. Furthermore, the only horizontal forces acting on the cable are located at the end points of the cable. Therefore, T_h is constant along the length of the cable. Cable tension can then be determined for any point along the cable,

$$T = T_h \sec(\Psi) \tag{5}$$

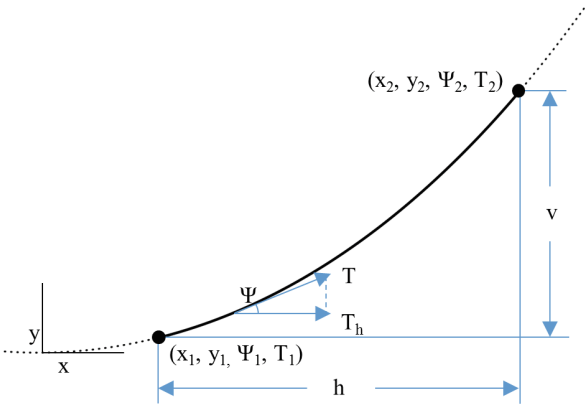

Fig. 2. Catenary curve profile

Solving (4) for Ψ, and substituting into (5),

$$T = T_h * \cosh\left(\frac{x}{A}\right) = A * w * \cosh\left(\frac{x}{A}\right) \tag{6}$$

For any given point in the field, the horizontal and vertical distances between the end-effector and the cable anchor point, h and v respectively, are known.

$$h = x_2 - x_1 \tag{7}$$

$$v = y_2 - y_1 = A * \cosh\left(\frac{x_1 + h}{A}\right) - A * \cosh\left(\frac{x_1}{A}\right) \tag{8}$$

Reducing the system of equations produces three equations with four unknowns, A, S, T1, and x1.

$$v = A * \cosh\left(\frac{x_1 + h}{A}\right) - A * \cosh\left(\frac{x_1}{A}\right) \tag{9}$$

$$S = A * \sinh\left(\frac{x_1 + h}{A}\right) - A * \sinh\left(\frac{x_1}{A}\right) \tag{10}$$

$$T_1 = A * w * \cosh\left(\frac{x_1}{A}\right) \tag{11}$$

2.2 Inverse Kinematics

Solving the inverse kinematics for CDPRs involves solving static equilibrium equations of the system. In the four-cable CDPR with a point-mass end-effector, there are

three translational degrees of freedom. The system is therefore defined by the equations for static equilibrium,

$$\sum \underline{F} = 0 = \sum_{i=1}^{4} \left(T_i * \underline{R_i}\right) - \underline{W} \tag{12}$$

Where T_i is the tension value of the *ith* cable, R_i is the unit vector in the direction of force $\underline{T_i}$, and W is the weight vector of the end-effector.

As indicated in the previous section, each cable is defined by a system of three equations that, given the current known geometric variables, depend on four unknowns. In the three-cable CDPR, adding the equations for three cables to the three static equilibrium equations produces a balanced system of equations that can be solved. Except in special circumstances, numerical methods must be used to solve the system as no explicit solution exists for this system of equations.

In the four-cable CDPR, there is one more unknown value than equilibrium equations available. The use of four cables in a three degree of freedom CDPR results in a redundant cable which generally suggests no unique solution exists for any given point in the system workspace. To solve this system of equations, a constrained optimization condition must be included with the problem. In this study, it was chosen to optimize the distribution of load on the cables by increasing the load on the lowest tension cable until the ratio between the highest and lowest tension is minimized. To achieve this, the model initially selects the position in the workspace to be considered. The length of the cable anchored the furthest away from the end-effector is then set to a predefined value greater than the straight-line distance between the anchor point and the end-effector. With one cable fully defined, the system of equations and unknowns are balanced, and can be solved iteratively. By increasing the tension on the prescribed cable, its tension gradually approaches that of the next lowest cable tension, more evenly distributing load between the cables until the system is considered optimized, and the resulting tensions, cable lengths, and cable profile are recorded.

2.3 Orientation Prediction

Thus far, the system end-effector has been assumed to be a point-mass. However, a potentially important parameter of CDPR design is the predicted orientation of the end-effector in different regions of the workspace. In the phenotyping system, end-effector orientation impacts the use of sensors intended to be downward facing as well as the range of motion of the end-effector gimbal.

Orientation is predicted by utilizing the force equilibrium results, applying them to a rigid body end-effector, and solving moment equilibrium equations,

$$\sum \underline{M} = 0 = \sum_{i=1}^{4} \underline{R_i} \times \underline{F_i} \tag{13}$$

where F_i is the force vector generated by the tension in the *ith* cable and R_i is the position vector from the center-of-mass of the end-effector to the attachment point of the *ith* cable. R_i is obtained by taking the position vector of the cable attachment point according to the end-effector frame of reference, R_i^*, and passing it through three rotation matrixes representing the rotation about the system x, y, and z axis.

$$[R]_x = \begin{bmatrix} 1 & 0 & 0 \\ 0 & \cos(\alpha) & -\sin(\alpha) \\ 0 & \sin(\alpha) & \cos(\alpha) \end{bmatrix} \tag{14}$$

$$[R]_y = \begin{bmatrix} \cos(\beta) & 0 & \sin(\beta) \\ 0 & 1 & 0 \\ -\sin(\beta) & 0 & \cos(\beta) \end{bmatrix} \tag{15}$$

$$[R]_z = \begin{bmatrix} \cos(\gamma) & -\sin(\gamma) & 0 \\ 0 & \sin(\gamma) & \cos(\gamma) \\ 0 & 0 & 1 \end{bmatrix} \tag{16}$$

$$R_i = [R]_{z''} * [R]_{y'} * [R]_x * R_i^* \tag{17}$$

The three moment equilibrium equations can be solved numerically for the three angles. With an orientation of the end-effector predicted, the force equilibrium[1] and moment equilibrium equations can be iteratively solved until the orientation prediction converges.

3 Theoretical Results

3.1 Simulator Outputs

The outputs of this model can be used to predict tension along the cables, cable lengths, cable profiles, and end-effector orientation. To accelerate simulation, it is assumed that system behavior is symmetrical across the geometric symmetry planes of the system. Thus, the same tension values are predicted in each quadrant of the field, but are associated with the mirrored cables.

Based on this assumption, cable tensions are solved across one quadrant of the workspace, and the behavior of the system in each other quadrant are then extrapolated. Figure 3a displays tension for a single cable as a function of end-effector position in the field at a fixed height.[2] Figure 3b illustrates the amount that the end-effector is predicted to tilt as a function of end-effector position in the field at a fixed height.

[1] After the first iteration of solving the force and moment equilibrium equations is performed, the end-effector is changed from a point-mass to a rigid body, oriented based on the prediction created by the results of the first iteration of moment equations.

[2] Data given for 68 kg end-effector, 3 m above ground.

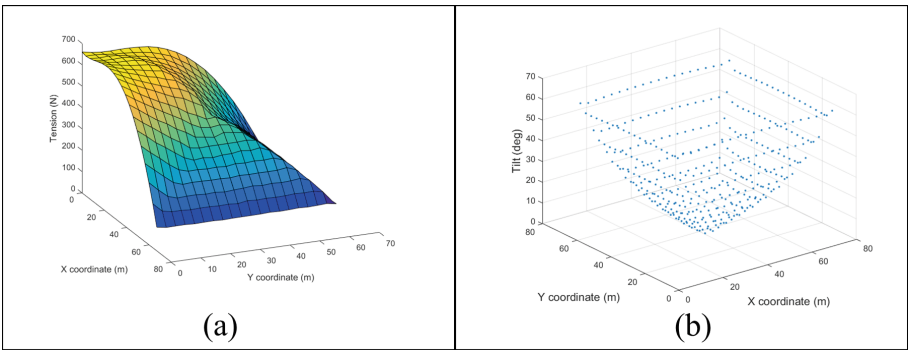

Fig. 3. (a) Theoretical cable tension. (b) Theoretical end-effector tilt

3.2 Dimensional Optimization

Modeling CDPRs requires knowledge of seven system parameters (Fig. 4):

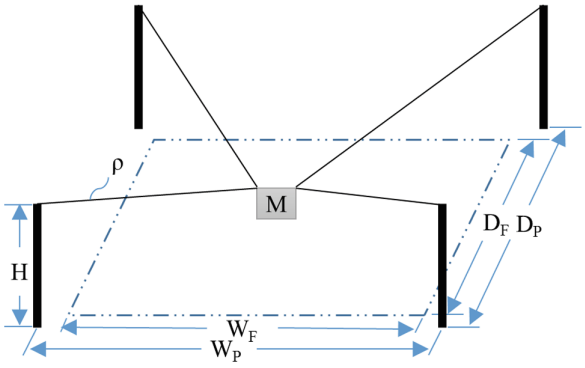

Fig. 4. System parameters of a four-cable CDPR system

- Field width, W_F
- Field depth, D_F
- End-effector mass, M
- Cable density, ρ
- Width between cable feed points, W_P
- Depth between cable feed points, D_P
- Height of cable feed points, H

Field dimensions and end-effector operational height were predetermined by the design of the phenotyping facility and are presented in Table 1. During system design, it was chosen to use a custom Kevlar cable with a fiber optic core for sensor data transmission. Use of the selected cable defines the cable density and adds an additional constraint by limiting tension in the cables.

Table 1. System parameters

Defined parameters		Variable parameters	
Field width	67 m	End-effector mass	45–90 kg
Field depth	60 m	Pole width	75–100 m
Maximum end-effector height	10 m	Pole height	15–26 m
Cable density	10 g/m		
Pole aspect ratio	10:9		
Maximum tension	1500 N		

The primary objective of this analysis is to determine the most appropriate location for the poles supporting the cable system and to determine the maximum required height for the cable-feed pulleys. The end-effector design is currently incomplete; therefore, studies investigating multiple end-effector weights are analyzed alongside of pole layout and height.

To optimize pole location and height as well as end-effector weight, three measurements must be analyzed:

- Maximum cable tension in consideration of cable strength
- Tension distribution in consideration of system stabilization
- End-effector orientation in consideration of end-effector reorientation capabilities

Many simulations were generated with different permutations of pole height, pole distancing, and end-effector mass. Selected results from these simulations are presented in Figs. 5 and 6. Figure 5 shows the influence of all three variables on the predicted maximum tensions for the system within the operational workspace.

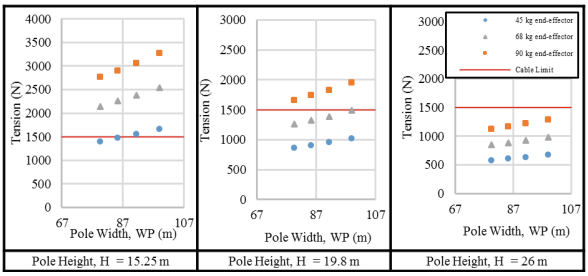

Fig. 5. Theoretical maximum tension in field

The even distribution of load between cables has a substantial impact on cable control and system vibrations [2]. The distribution of load between the cables can be parameterized by the variable η as follows:

$$\eta_{xyz} = \frac{T_{max}(x, y, z)}{T_{min}(x, y, z)} \tag{18}$$

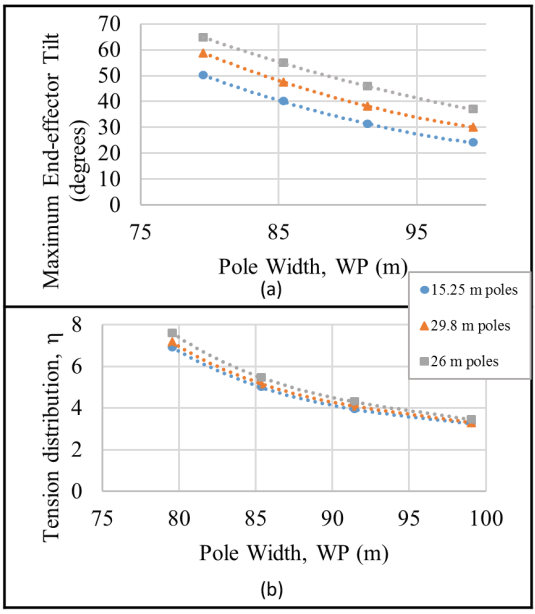

Fig. 6. (a) Theoretical end-effector tilt (b) Theoretical tension distribution

Where T_{max} and T_{min} are the highest and lowest cable tensions, respectively, for the given orientation. η_{max} is then the highest predicted η_{xyz} in the workspace for the given system configuration. Load distribution, and therefore cable performance, is expected to improve as η_{max} approaches one. Figure 6b shows the impact of pole location and height on η_{max}.[3]

As the end-effector moves radially from the center of the workspace, the uneven distribution of load on the cables causes the vertical axis of the end-effector to tilt towards the center of the field, away from the vertical axis of the workspace (Fig. 3b). This behavior can be parameterized by measuring the angle between the vertical axis of the end-effector and the vertical axis of the workspace. For a gimbaled end-effector, which is what is being used in this project, the maximum predicted angle is required to determine the required range of motion of the gimbal. In an end-effector without a gimbal, extreme angles can limit the use of sensors and equipment that are required to maintain a certain orientation. Figure 6a shows the impact of pole location and height on the end-effector inclination angle.[4]

According to preliminary designs, the end-effector with the maximum weighted sensor package will be between 45 and 68 kg. Based on the data presented in Figs. 5 and 6, the minimal system configuration that will safely support a 68 kg end-effector utilizes 19.8 m (65 ft) poles. A pole shorter than this would require placement too close to the workspace and cable performance would likely cause the system to be

[3] End-effector weight was found to have no impact on η_{max}.

[4] End-effector weight was found to have no impact on end-effector inclination angle.

uncontrollable. Taller poles reduce the load on the cables, which allow the poles to be placed further from the workspace, improving cable performance and reducing end-effector tilt. However, this introduces further design challenges. Moving the poles outwards expands the space requirements of the system by adding a large perimeter of empty space between the workspace and poles. Also, taller poles are more expensive and require larger footings for support.

With 19.8 m poles selected, the maximum allowable width between poles for the specified end-effector weight and cable strength is 99 m (325 ft). Positioning the poles this far from the workspace increases system footprint by 53% and generates an 18% increase in maximum tension compared to a system with similar poles placed 80 m apart. However, it also reduces η and end-effector inclination by 54% and 49% respectively, enhancing system performance. Positioning the poles any further out, however, increases cable tension, reducing the safety factor for the cables. The final recommended configuration for this system is outlined in Table 2.

Table 2. Optimized system dimensions

Parameter	Optimized dimension
Pole distance	99 × 89 m (325 × 293 ft)
Pole height	19.8 m (65 ft)
End-effector mass limit	68 kg (150 lb)

4 Experimental System

4.1 Design

A twelfth-scale model of the field phenotyping system was designed to confirm the simulator results and to test control system design, system dynamics, and end-effector stabilization hardware and controls. Scaling factors are calculated using the Buckingham Pi theory following the procedures used by Yao, et al. [2]. Dimensional Parameters are listed in Table 3 (Fig. 7).

Table 3. Scaled system parameters

Parameter	Similarity scale	Full size dimension	Model dimension
Field width	1:12	67 m	5.60 m
Field depth	1:12	60.35 m	5.03 m
Pole height	1:12	25.91 m	2.16 m
Cable density	1:55*	10.8 g/m	0.197 g/m
End-effector weight	1:144	77 kg	0.535 kg

An appropriate cable was not utilized in the twelfth-scale system due to the challenges of scaling cable properties of density, construction, and stiffness. Dyneema fishing line with a diameter of 1 mm was instead used. Due to this change, cable sag and stiffness are not similar between the twelfth-scale and full-scale systems. Thus,

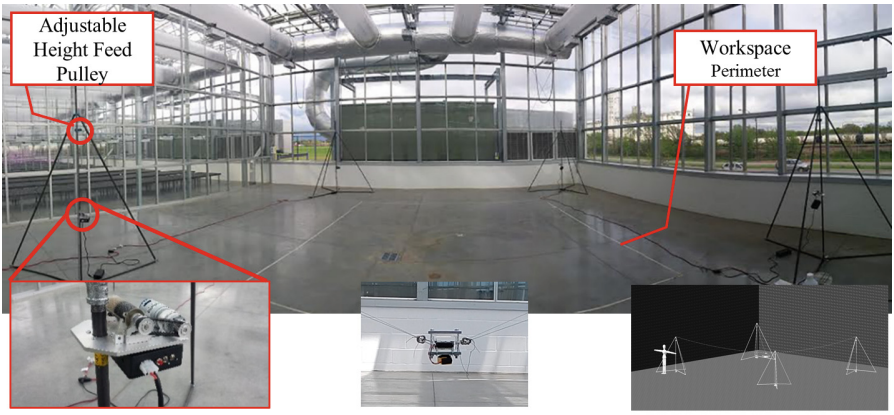

Fig. 7. Twelfth-scale system

full-scale system dynamics cannot be predicated on twelfth-scale experimentation. As a result, the twelfth-scale system is used in studying *general* CDPR behavior in the testing of stabilization and control systems. While these tests may be briefly mentioned, their results are not discussed in this paper.

The twelfth-scale system was designed to test, not only the determined optimal configuration, but an array of system configurations. As such, poles used to support the cable system were designed as collapsible tripods to allow for easy alteration to pole layouts and system scales. Cable-feed pulleys with adjustable height were mounted on the poles to experiment with multiple cable systems heights. Attached to the poles were custom winches to actuate cable feed. Each winch wirelessly communicated with the system navigational controller to drive the system with motor-mounted-encoder feedback to track cable length and approximate end-effector position.

An end-effector mounted with an inertial measurement unit (IMU) was created to measure end-effector orientation when navigated through the workspace. It was also used to observe the response to impulse disturbances on the end-effector as well as the impact of end-effector acceleration during travel on system vibration. Additionally, a gimballed end-effector equipped with load cells at the cable connection points was used to perform experiments to measure cable tensions during travel as well as to confirm tension predictions from the simulator.

4.2 Experimental Static Results

One task of the twelfth-scale system was to determine the accuracy of the mathematical model. Two primary criteria for confirming the validity of the simulator results were cable tension and end-effector orientation. Two tests were performed to determine the accuracy of the theoretical predictions. One test involved navigating the load-cell

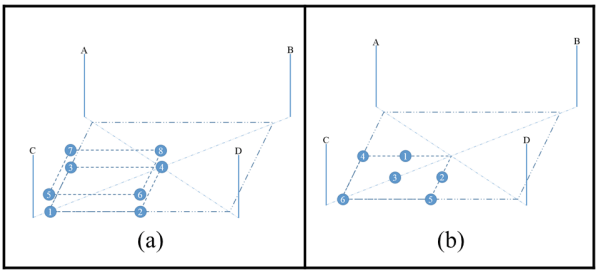

Fig. 8. (a) Tension experiment tested locations (b) Orientation experiment tested locations

end-effector through a series of points (Fig. 8a).[5] At each point, load cell readings were taken and were compared to theoretical values predicted by the simulator, as displayed in Fig. 9.[6] The second test involved navigating the IMU end-effector through a series of points (Fig. 8b) to measure end-effector orientation, which in turn was compared to simulator results, as displayed in Fig. 10. Due to the symmetry of the system, all tests are performed in one quadrant of the workspace, and the results are assumed to mirror across the symmetry planes.

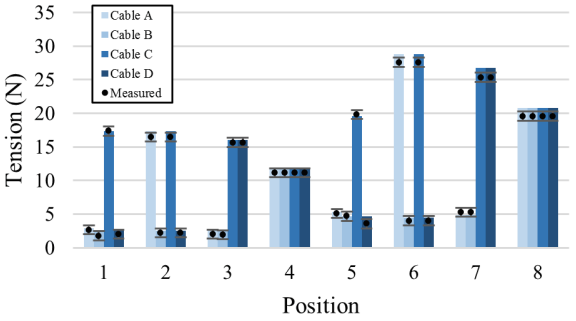

Fig. 9. Theoretical vs. experimental values of the cable tension. The bars indicate the theoretical values and the circles are the means of the measured values from the 12th-scale model. Error bars are one standard deviation of the mean.

Results from the first test show that the simulator predicted cable tensions to within an error of 0.7 N with a standard deviation of 0.5 N for an end-effector of weight 18.35 N. Results from the second test were then shown to predicted end-effector tilt to within 2.0° with a standard deviation of 1.3°. These results indicate that the designed simulator accurately predicts cable performance for the purpose of static analysis.

[5] For tension testing, points are located at heights of 0.25 m (lowest feasible elevation for given end-effector) and 1.14 m (maximum safe operating height for given weight).

[6] Rather than using a 0.535 kg end-effector for the tension tests, a 1.9 kg end-effector was used. This was done to increase cable tensions to a level more appropriate for the utilized load cells.

Based on these experiments, agreement between the simulator and physical model is adequate to justify the use of the simulator results in predicting the static behavior of the full-scale phenotyping system.

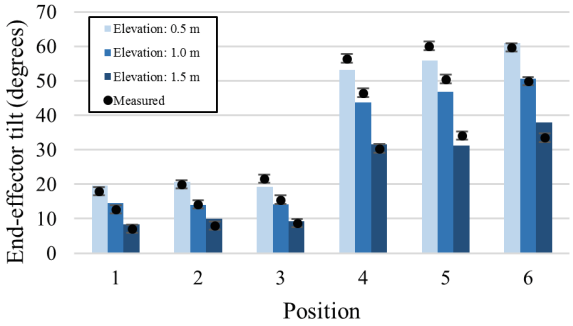

Fig. 10. Theoretical vs. experimental values of the end-effector tilt angle. The bars indicate the theoretical values and the circles are the means of the measured values from the 12th-scale model. Error bars are one standard deviation of the mean.

5 Conclusions

This paper addressed the rationale for use of a cable-driven parallel robot (CDPR) system for control of an outdoor phenotyping site. It addressed the derivation and solution of the inverse kinematics and used this model to optimize system dimensions. These simulations were compared against experimental results of a twelfth-scale system to determine the accuracy of the calculations. This research can be extended to aid in modeling of the dynamic system to predict system vibrations and to determine stabilization requirements during system control. This research can readily be adapted for other four-cable CDPR systems to predict static properties.

References

1. Hiller, M., Fang, S., Mielczarek, S., Verhoeven, R., Franitza, D.: Design, analysis and realization of tendon-based parallel manipulators. Mech. Mach. Theory **40**(4), 429–445 (2005)
2. Yao, R., Tang, X., Wang, J., Huang, P.: Dimensional optimization design of the four-cable-driven parallel manipulator in FAST. IEEE ASME Trans. Mechatron. **15**(6), 932–941 (2010)
3. Kawamura, S., Choe, W., Tanaka, S., Pandian, S.R.: Development of an ultrahigh speed robot FALCON using wire drive system. In: 1995 Proceedings of the IEEE International Conference on Robotics and Automation, vol. 1, pp. 215–220 (1995)
4. Zi, B., Duan, B.Y., Du, J.L., Bao, H.: Dynamic modeling and active control of a cable-suspended parallel robot. Mechatronics **18**(1), 1–12 (2008)

5. Fang, S., Franitza, D., Torlo, M., Bekes, F., Hiller, M.: Motion control of a tendon-based parallel manipulator using optimal tension distribution. IEEE ASME Trans. Mechatron. **9**(3), 561–568 (2004)
6. Suilu, Y., Zhao, W., Qi, L., Yixin, C.: Stiffness analysis of a wire-driven parallel manipulator. In: 2012 IEEE International Conference on Computer Science and Automation Engineering (CSAE), vol. 3, pp. 31–34 (2012)
7. Yamamoto, M., Yanai, N., Mohri, A.: Trajectory control of incompletely restrained parallel-wire-suspended mechanism based on inverse dynamics. IEEE Trans. Robot. **20**(5), 840–850 (2004)
8. Bin, L., Yinghui, L., Xuegang, Y.: Dynamic modeling and simulation of flexible cable with large sag. Appl. Math. Mech. **21**(6), 707–714 (2000)
9. Kozak, K., Zhou, Q., Wang, J.: Static analysis of cable-driven manipulators with non-negligible cable mass. IEEE Trans. Robot. **22**(3), 425–433 (2006)
10. Russell, J.C., Lardner, T.J.: Statics experiments on an elastic catenary. J. Eng. Mech. **123** (12), 1322–1324 (1997)
11. Nan, R., Li, D., Jin, C., Wang, Q., Zhu, L., Zhu, W., Zhang, H., Yue, Y., Qian, L.: The five-hundred-meter aperture spherical radio telescope (FAST) project. Int. J. Mod. Phys. D **20**(6), 989–1024 (2011)
12. Costello, E.: Length of a hanging cable. Undergrad. J. Math. Model One Two 4(1) (2011)
13. Yingjie, L., Wenbai, Z., Gexue, R.: Feedback control of a cable-driven gough-stewart platform. IEEE Trans. Robot. **22**(1), 198–202 (2006)
14. Yang, G., Pham, C.B., Yeo, S.H.: Workspace performance optimization of fully restrained cable-driven parallel manipulators. In: 2006 IEEE/RSJ International Conference on Intelligent Robots and Systems, pp. 85–90 (2006)
15. Maeda, K., Tadokoro, S., Takamori, T., Hiller, M., Verhoeven, R.: On design of a redundant wire-driven parallel robot WARP manipulator. In: 1999 Proceedings of the IEEE International Conference on Robotics and Automation, vol. 2, pp. 895–900 (1999)
16. Ebert-Uphoff, I., Voglewede, P.A.: On the connections between cable-driven robots, parallel manipulators and grasping. In: 2004 Proceedings of the IEEE International Conference on Robotics and Automation, ICRA 2004, vol. 5, pp. 4521–4526 (2004)
17. Shen, Y., Osumi, H., Arai, T.: Manipulability measures for multi-wire driven parallel mechanisms In: Proceedings of the IEEE International Conference on Industrial Technology, pp. 550–554 (1994)
18. Voglewede, P.A., Ebert-Uphoff, I.: Measuring 'closeness' to singularities for parallel manipulators. In: 2004 Proceedings of the IEEE International Conference on Robotics and Automation, ICRA 2004, vol. 5, pp. 4539–4544 (2004)